REVIEW PAPER

'In vivo' optical approaches to angiogenesis imaging

**T. J. A. Snoeks · C. W. G. M. Löwik ·
E. L. Kaijzel**

Abstract In recent years, molecular imaging gained significant importance in biomedical research. Optical imaging developed into a modality which enables the visualization and quantification of all kinds of cellular processes and cancerous cell growth in small animals. Novel gene reporter mice and cell lines and the development of targeted and cleavable fluorescent "smart" probes form a powerful imaging toolbox. The development of systems collecting tomographic bioluminescence and fluorescence data enabled even more spatial accuracy and more quantitative measurements. Here we describe various bioluminescent and fluorescent gene reporter models and probes that can be used to specifically image and quantify neovascularization or the angiogenic process itself.

Keywords Angiogenesis · Bioluminescence · Fluorescence · Molecular imaging · Optical imaging

Introduction

Optical imaging

Optical imaging is a very versatile, sensitive and powerful tool for molecular imaging in small animals. It is based on the detection of photons in the visible light spectrum emitted from living cells, tissues or animals and can be divided in two main modalities, bioluminescence imaging (BLI) and fluorescence imaging (FLI). Optical imaging of

T. J. A. Snoeks · C. W. G. M. Löwik (✉) · E. L. Kaijzel
Department of Endocrinology, Leiden University Medical
Center, Building 1, C4-R86, Albinusdreef 2,
2333ZA Leiden, The Netherlands
e-mail: c.w.g.m.lowik@lumc.nl

angiogenesis and existing vasculature is currently dominated by FLI-based imaging models, but there are several interesting BLI models as well. This review provides an overview of the available optical imaging models that can be used within angiogenesis related research.

Bioluminescence imaging

Bioluminescence imaging has been developed over the last decade as a tool for molecular imaging of small laboratory animals, enabling the study of ongoing biological processes such as tumor growth and metastasis and gene expression in vivo [1]. All bioluminescent reporter systems are based on the detection of photons produced in an enzymatic reaction in which a substrate, like luciferin or coelerentarazin, is oxidized by an enzyme, luciferase. There are many different kinds of luciferases occurring in nature and being adapted for research. The most commonly used luciferase for molecular imaging purposes is the one extracted from the North American firefly (Photinus pyralis; FLuc) emitting light with a broad emission spectrum and a peak around 560 nm but other useful luciferases have also been cloned from corals (Tenilla), jellyfish (Aequorea), several bacterial species (Vibrio fischeri, V. harveyi) and red or green click beetle (Pyrophorus plagiophthalamus) which have been optimized to produce green–orange (544 nm) or red (611 nm) light after oxidizing luciferin.

Luciferases from the anthozoan sea pansy (Renilla reniformis) and the marine copepod (Gaussia princeps) react with coelenterazine and are ATP-independent to produce blue light with peak emission at approximately 480 nm. Despite the blue emission wavelength of these enzymes, limited biodistribution and rapid kinetics of coelerentarazin in small animals, these luciferases have been proven very useful for in vivo applications for

molecular imaging [2–6]. Because the substrates luciferin and coelentarazin for firefly luciferase (FFluc) and Gaussia luciferase (Gluc), respectively, show no crossreactivity, concomitantly imaging of distinct cell populations that either express FFluc or Gluc can be performed within the same animal.

BLI reporter systems are especially suitable for biomedical research purposes due to the extremely low background signal, high signal to noise ratio, non-invasive character, short acquisition time (seconds to minutes) and the possibility to measure more animals at once (high throughput).

Fluorescence imaging

In contrast to BLI, fluorescence imaging is not based on the production of photons by an enzymatic reaction; instead, a fluorescent compound (fluorophore) can be exited by photons of a certain wavelength from an external light source. Upon relaxation to its ground state, the fluorophore emits photons at a different wavelength. These emitted photons are the signal which is used for imaging. Similar to BLI, whole body FLI enables tracking of tumor growth and metastasis, gene expression, angiogenesis and bacterial infection, quantitatively (reviewed in Hoffman [7]).

There is a wide range of fluorophores available, ranging from fluorescent dyes and nanoparticles, like quantum dots, to fluorescent proteins which can be expressed in transgenic models. Each fluorophore has several characteristics amongst which the excitation wavelength, emission wavelength and quantum yield or brightness. The excitation wavelength is the optimal wavelength of external light to bring the fluorophore to its exited state. The emission wavelength is the wavelength of the photons emitted upon relaxation. Usually, the emitted photons have a longer wavelength than the photons used for excitation and thus, the emitted photons have a lower energetic value. The brightness or quantum yield of a fluorophore is defined by the fraction of molecules that emit a photon after direct excitation by the excitation light source. In most cases this value is nearly the same value as the ratio between the number of photons emitted from a bulk sample and the total number of absorbed photons [8]. All three of these properties, excitation wavelength, emission wavelength and quantum yield, have important implications for the use of a certain fluorophore for imaging [9].

When using fluorescence for in vivo imaging, tissue absorbance, scattering and auto-fluorescence can become a problem especially when imaging structures deeper in the animal. Most auto-fluorescence occurs in the green part of the spectrum [9, 10]. The amount of auto-fluorescence rapidly decreases when shifting towards a longer excitation wavelength, the red parts of the spectrum. Near infrared

(IR) light causes hardly any auto-fluorescence [10–12]. Moreover, light penetration, tissue absorption and scattering are greatly reduced at the near infrared end of the spectrum compared to green light.

Recently fluorescent proteins with increasingly longer emission maxima (up to 649 nm), like the series of red shifted proteins obtained by mutating dsRed, i.e., mFruits like mCherry, mTomato and mPlum [13, 14], and a series of recently developed very bright, red-shifted proteins derived from the anemone Entacmaea quadricolor like Katushka and mKate [12], have been developed. The longer emission wavelengths lead to a reduction of background auto-fluorescence and substantially increase tissue penetration. Moreover, the newest generation of mammalian expressed fluorescent proteins, based on bacterial phytochromes, enter the near infrared with emission spectra exceeding wavelengths of 700 nm [15].

Both luciferase for BLI and various fluorescent proteins for FLI can be expressed in cells or animals. Using specific promoters to drive reporter gene expression, these imaging modalities can be used not only for localization but can also provide functional information.

Whole body optical imaging instruments

In the last decade there has been a rapid growth of optical imaging applications in small animal models driven by creative approaches to apply these techniques in biomedical research and also by the availability of innovative instruments. Most of the BLI imaging systems provide 2-dimensional planar information in small animals, showing the locations and intensity of light emitted from the animal in pseudo-color scaling. Nowadays, there are many commercial whole-body pre-clinical BLI systems on the market.

However, in its planar projection form, BLI is non-quantitative and its spatial resolution is relatively poor. Interestingly, recent developments in bioluminescence tomography promise to provide three dimensional quantitative source information with improved spatial resolution [16–18].

BLI imaging systems that are able to image moving objects have been developed for experiments in which anesthesia is a problem. Examples of such real time imaging systems are the IVIS Kinetic (Caliper Life Sciences Inc.) and the Photon Imager (Biospace Lab) [19, 20].

In analogy with BLI technology, the vast majority of applications of in vivo small animal fluorescence imaging are based on planar epi-illumination imaging. However, an important part of the research conducted in whole-body small animal imaging is concerned with the development of novel fluorescence tomography approaches pushing

further the limits of the modality in terms of sensitivity, quantification and spatial resolution [21].

New FLI systems are able to capture spectral information of each pixel of an image. The spectral information can be unmixed to reveal all the different spectra that, taken together, form the actual image. By doing so, it is possible to identify multiple fluorescent labels within an image and to remove background (auto-)fluorescence. This way of analyzing spectral data within fluorescence datasets is called spectral unmixing [22, 23].

Gene reporter systems

Whole body imaging of VEGF signaling

VEGF is one of the key factors regulating angiogenesis. Most of the vasculogenic and angiogenic effects of VEGF are mediated through the VEGF receptor 1 (VEGFR1, FLT-1) and VEGF receptor 2 (VEGFR2, Flk-1) expressed on endothelial cells [24]. During angiogenesis, including tumor angiogenesis, both VEGF and VEGFR2 expression are locally upregulated [25–28]. VEGF receptors and VEGF itself are attractive targets for molecular imaging given their important role and upregulated expression during (tumor) angiogenesis. As a result, several models have been developed to image and quantify VEGF receptor and VEGF expression.

To monitor VEGFR2 gene expression in vivo as a read-out for angiogenesis, in real time, Zhang et al. [29] developed a VEGFR2-luciferase transgenic mouse model (FVB/N-Tg(VEGFR2-luc)-Xen). In this mouse, luciferase expression is under control of the VEGFR2 promoter region [30] causing endothelial cells lining the angiogenic blood vessels to express luciferase. The VEGFR2-luc mouse has been validated using cutaneous wound healing models in which VEGFR2 expression was upregulated at the site of a punch wound marked by a clear localized increase of the luciferase signal. The increase in VEGFR2 gene activation reached a maximum after 7–10 days after the wound was inflicted [29]. These findings were consistent with later studies which used the same mouse model [31, 32].

Co-registration of BLI and FLI makes it possible to follow multiple processes in one mouse, for instance tumor growth and angiogenesis. As an example, we used the murine breast cancer cell line SMF [33] and the VEGFR2-luc knock-in mouse [29]. A VEGFR2-luc knock-in mouse received an orthotopic inoculation with red fluorescent SMF-mCherry breast cancer cells (right side of the animal) and wild type SMF cells (left side of the animal. The fluorescent signal from the SMF-mCherry cells and bioluminescent signal from the locally upregulated VEGFR2

expression enabled the simultaneous imaging and quantification of angiogenesis and tumor growth real time in vivo. We show the increase in tumor size from week 2 to week 4 using FLI. The FLI signal is only detected at the site of the fluorescent tumor, not at the site with the wild type tumor. The pro-angiogenic response is visualized with BLI both at the site of the fluorescent tumor as well as the site with the wild type tumor (Fig. 1). This way, both tumor growth and pro-angiogenic signaling can be quantified simultaneously, the ratio of which can be used as a measure for angiogenic characteristics of certain tumors.

Other in vivo approaches to study VEGF signaling and angiogenesis in real time are transgenic mouse models which express green fluorescent protein (GFP) or luciferase driven by the VEGF promoter, namely the fluorescent VEGF/GFP [34] and the bioluminescent pVEGF-TSTA-fl transgenic models [35]. The latter approach makes use of the GAL4-VP16 two step transcriptional amplification (TSTA) system [36] to amplify luciferase expression. In this system, the full length human VEGF promoter is placed upstream of the gene encoding a GAL4-VP16 fusion protein. This fusion protein binds GAL4 binding sites that are placed upstream of an adenovirus E4 TATA minimal promoter. This promoter drives luciferase gene expression resulting in GAL4-induced luciferase expression [35]. The extra step via GAL4-VP16 leads to an amplification in luciferase expression. The TSTA system has been used previously shown to amplify prostate specific luciferase expression leading to a 50-fold increase compared to the direct, one step system [36].

Wang et al. [35] demonstrated the correlation between VEGF expression and BLI signal both in vitro and in vivo. In addition, they showed that this transgenic animal can be used to study the VEGF response in both wound healing assays as well as tumor growth models (Fig. 2).

In vivo imaging of vasculature

The VEGF and VEGFR2 reporter mice make it possible to image the areas in which there is an increased pro-angiogenic and vasculogenic signaling. Other transgenic animal models have been developed to image the actual existing vasculature. These models include several transgenic animals with endothelial specific expression of fluorescent proteins like GFP, e.g., the Tie2-GFP mice [37, 38] and the eNOS-GFP mouse [39]. The GFP models are well suited for in vivo microscopic and confocal approaches in contrast to the whole body optical imaging models discussed above.

The Tie2-GFP nude mouse expresses GFP under direction of the endothelial specific receptor tyrosine kinase (Tie2). This mouse is well suited to study angiogenesis and interactions between various (human) tumor
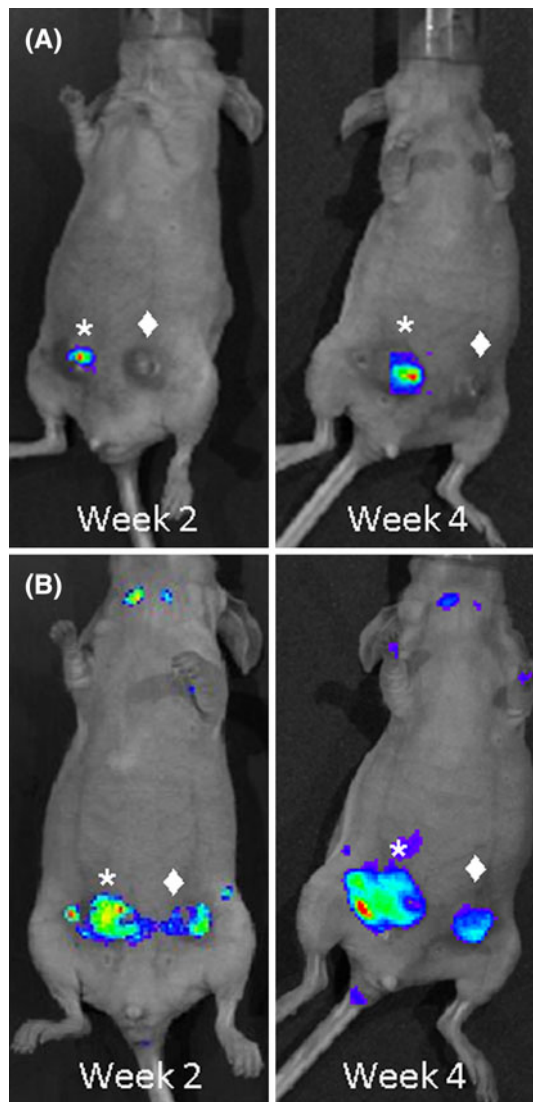
Fig. 1 Multi-modality imaging of tumor growth and angiogenesis. A VEGFR2-luc knock-in mouse was orthotopically, i.e., in the mammary fat pad, inoculated with 1×10^6 SMF-mCherry cells (marked with *asterisk*) and SMF wild-type cells (marked with *filled diamond*), a murine breast cancer cell line. SMF-mCherry cells constitutively express the far *red* fluorescent protein mCherry, which accumulates in the cytoplasm. Mice were imaged at week 2 and week 4 both FLI (**a**) and BLI (**b**) using the IVIS Spectrum (Caliper LifeSciences, USA) camera system. **a** Tumor growth of the mCherry positive tumor could be followed over time using FLI. **b** The BLI signal was present at the site of both the mCherry positive and negative tumors indicating a local upregulation of VEGFR2 expression and tumor angiogenesis. (Snoeks et al. unpubl. results)

xenografts and tumor vasculature in vivo due to its athymic nude background. The non-invasive character of fluorescence imaging allows follow up over time and assessment of anti-angiogenic treatment efficacy in vivo (Fig. 3) [37].

The eNOS-GFP. mouse expresses GFP driven under the endothelial specific promoter of endothelial nitric oxide synthase (eNOS) [3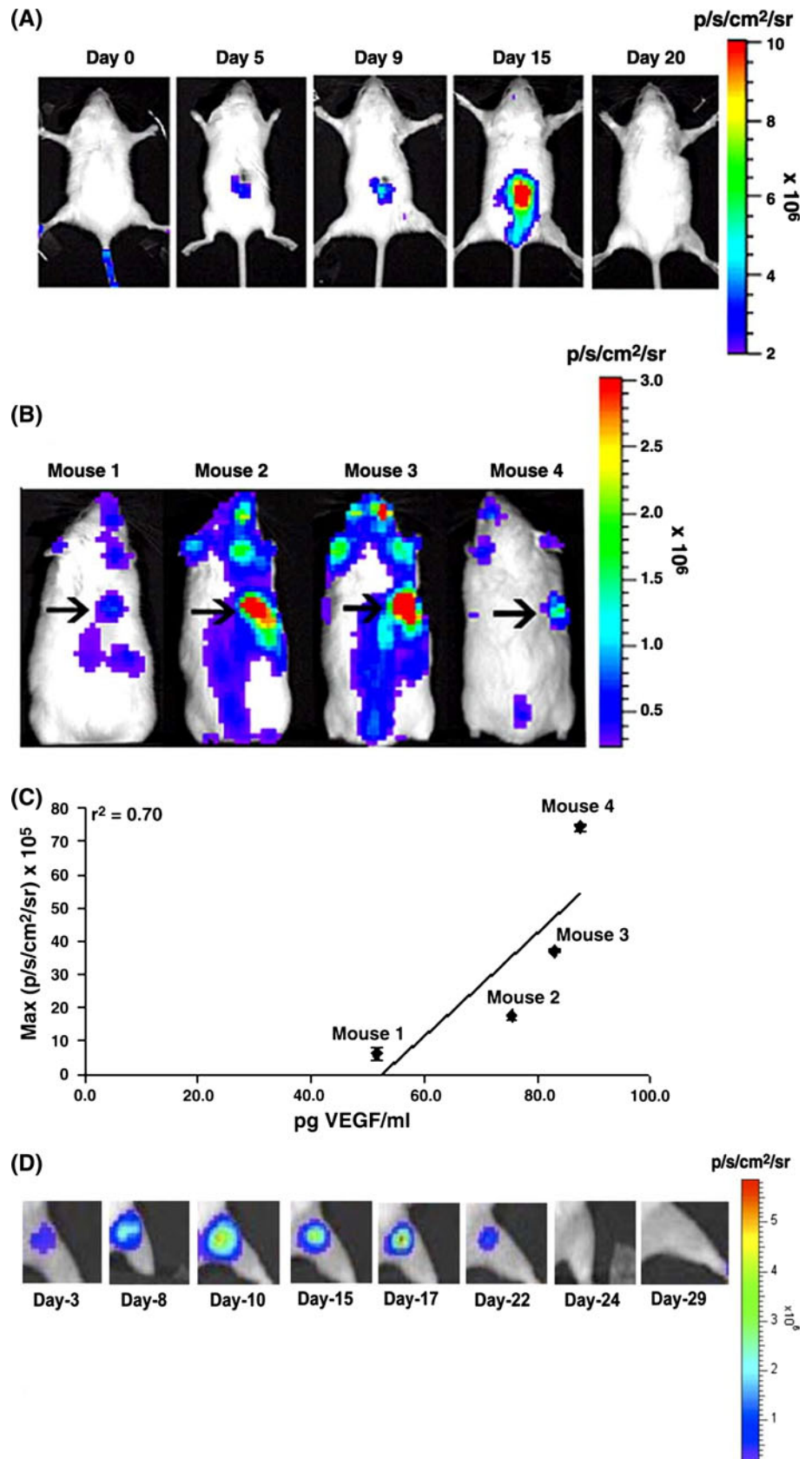9]. A dorsal skinfold chamber can be used to visualize the interaction between tumor cells and growing vasculature. In such a setup, the skin on the back of a mouse is stretched and fitted between two glass slides allowing in vivo microscopy. When SMF-mCherry cells are inoculated between these glass slides, confocal microscopy allows the fluorescent imaging of both tumor growth (mCherry) and developing tumor vasculature (GFP) in such a dorsal skin-fold chamber (Fig. 4).

Yang et al. [40] used wild type mice and GFP positive tumor xenografts to follow tumor angiogenesis in real time. The blood vessels appear as dark contrast against the bright fluorescent tumor. This way they were able to image, quantify and follow the vessel density in orthotopically transplanted tumors over time either by whole body imaging or intravital examination. In a similar approach, dual-color imaging of red fluorescent tumor xenografts in a mouse expressing GFP driven by the chicken β-actin promoter and cytomegalovirus enhancer [41] was demonstrated [42]. In this model the tumor vasculature and other host-derived stromal cell types such as fibroblasts appear in green within the red fluorescent tumor [41].

Another transgenic mouse model to study angiogenesis and nascent vasculature is the GFP mouse in which GFP expression is driven by the regulatory elements of the nestin gene. Nestin is a marker for neural stem cells, neural progenitor cells and neuro-epithelial stem cells [43]. This so-called nestin regulatory element–driven-GFP (ND-GFP) mouse was originally developed in order to study the self renewal capabilities of neural stem cells and progenitor cells [43–45]. In addition to neural cell types, nestin is expressed in the hair follicular bulge as well [46]. During the murine hair cycle, pronounced vascular remodeling occurs with more than a fourfold increase in perifollicular vessel size [47]. It has been found in the ND-GFP mouse that besides the follicular bulge, the perifollicular nascent blood vessels were GFP and thus nestin positive [48, 49]. By transplanting follicles from the ND-GFP mice into nude mice it became clear that follicle derived cells gave rise to these newly formed perifollicular blood vessels. The perifollicular blood vessels connected with the existing vasculature of the receiving animal. Moreover, the newly formed GFP positive vessels expressed the endothelial cell specific marker CD31 confirming that these vessels were indeed blood vessels [48]. In addition, it has been shown that follicle derived vessel growth was increased near wounded skin and that the GFP positive vessels grew from the transplanted follicle towards the wound [48]. Later studies have confirmed the ND-GFP mouse can be used as a model to image nascent tumor vasculature in the skin, mammary fat pad, pancreas, liver, lung, bone and colon [50–55].

One of the most recent mouse models, the Tie-2-Biotag mouse, makes use of the highly specific and strong binding

Fig. 2 Induction of *fl* expression during wound healing in a pVEGF-TSTA-*fl* transgenic mouse. **a** mouse was imaged before wound creation in the CCD camera (day 0) and imaged again subsequent to wound creation every 4–5 days using D-luciferin (150 mg/kg ip). **b** Optical CCD images of four pVEGF-TSTA-*fl* transgenic mice (mice 1–4) on days 19, 20, 21, and 22 after creation of the wound. *Arrows* indicate the position of the wounds. **c** Correlation plot of maximum bioluminescence signal ($p \cdot s^{-1} \cdot cm^{-2} \cdot sr^{-1}$) vs. endogenous VEGF levels in the wound tissue ($r^2 = 0.70$). *Error bars* represent the standard error for triplicate samples in the ELISA assay. (d) pVEGF-TSTA-*fl* transgenic mice were injected subcutaneously with 5×10^6 NK2 (FVB/N mouse mammary tumor cell line) cells in the *lower right* flank. Mice were imaged on day 4 and subsequently every few days until day 29 using D-luciferin as the reporter substrate (150 mg/kg, injected ip). CCD camera imaging revealed a detectable bioluminescence signal in the area around the tumor on day 4. Signal intensity continued to increase until day 17, after which a considerable decline in signal was observed (days 22–29). (Adapted with permission from Wang et al. Physiol Genomics. 2006 Jan 12; 24(2):173–80. [35])
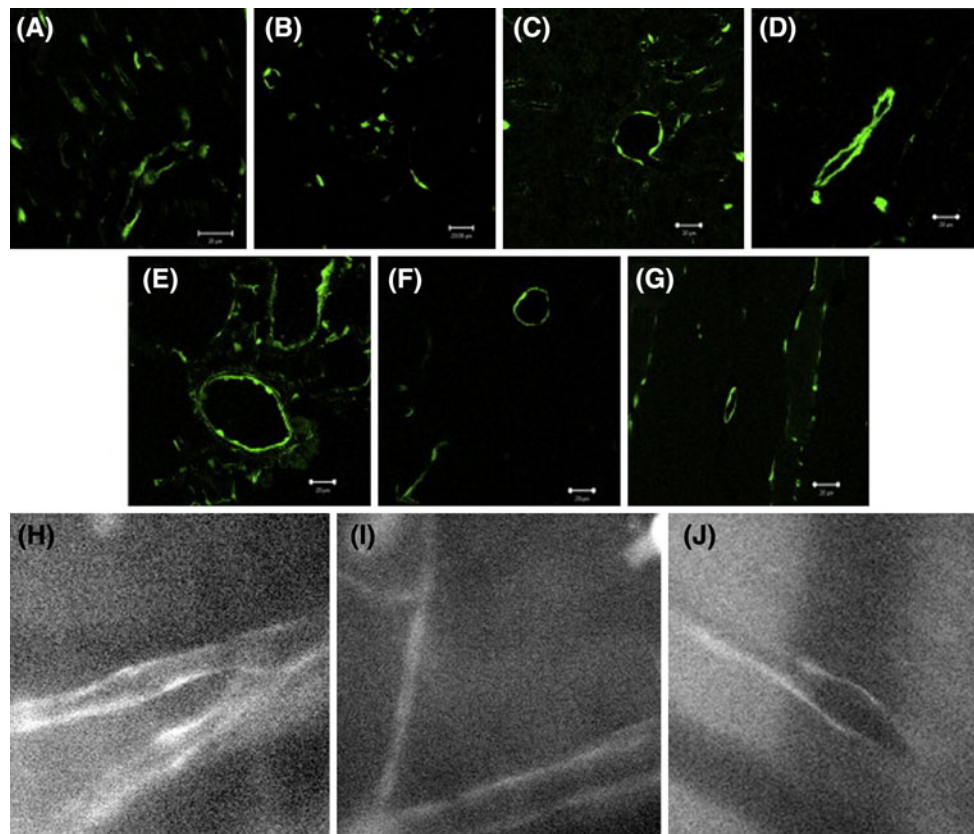
Fig. 3 GFP vessels in the athymic Tie2-GFP transgenic adult mouse. **a–g** Images from heart, kidney, liver, spleen, lung, brain, and calf muscle, respectively. *Scale bar* represents 20 μm. **h–j** Intr. avital fluorescence microscopy images of GFP vessels in the muscle (**h–i**) and in the ear skin (**j**). (Reprinted from Hillen F, Kaijzel EL, Castermans K, oude Egbrink MG, Lowik CW, Griffioen AW. A transgenic Tie2-GFP athymic mouse model; a tool for vascular biology in xenograft tumors. Biochem Biophys Res Commun 2008; 368:364–7. [37])
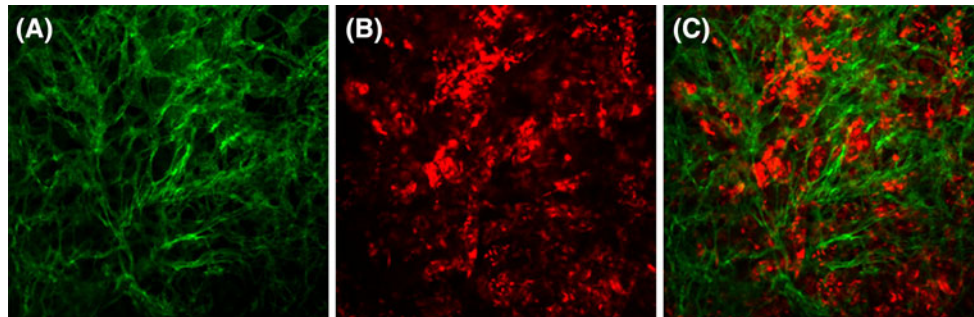

Fig. 4 In vivo fluorescent microscopy of tumor vasculature. An eNOS-GFP mouse received a subcutaneous inoculation with 1×10^6 SMF-mCherry cells in a dorsal skinfold chamber. Images were taken using a Zeiss CLSM 510 Meta microscope with a 10× objective. The following excitation lasers and emission filters were used, *green*: laser 488 nm, filter BP 505–550 nm, *red*: laser 543 nm, filter BP 560–615 nm. **a** Green fluorescent vasculature. **b** *Red* fluorescent tumor-cells. **c** Superimposed images of the vasculature and tumorcells (Kaijzel, Ten Hagen et al. unpubl. results)

of avidin to biotin, commonly used in immunohistochemical staining techniques. In order to do so, this mouse expresses Biotin Ligase (BirA) and a cluster of BirA substrate sequences (Biotags) fused to a transmembrane domain under control of the endothelial cell specific Tie2 promoter. Cells expressing this Biotag-BirA cassette can be targeted in vivo with avidinated probes of choice. These transgenic mice, in which vascular endothelial cells are biotinylated already during angiogenesis, are highly useful for targeted in vivo imaging of angiogenesis and established vasculature using avidinated agents suitable for any desired imaging modality [56].

Optical imaging of hypoxia

Hypoxia and the subsequent stabilization of hypoxia inducible factor-1 (HIF-1) is one of the key initiators of (tumor-)angiogenesis as reviewed by Liao and Jonson [57]. In short, HIF-1 has an oxygen dependent degradation domain (ODD) which is hydroxylated in an oxygen dependent manner by prolyl hydroxylases. As a result, the ODD binds the Von Hippel-Lindau factor (VHL) under normoxic conditions, targeting HIF-1 for proteasomal degradation. VHL cannot bind HIF-1 under hypoxic conditions, leading to stabilization of HIF-1 and downstream signaling [58].

The promoter regions of most genes upregulated under hypoxic conditions, amongst which VEGF, contain a hypoxia responsive element (HRE). This HRE is the HIF-1 target binding site [59]. To enable real time measurement of both in vivo as well as in vitro HIF-1 activity several reporter constructs have been developed in which reporter gene expression such as luciferase [60–62] or GFP [63, 64], is driven by HREs. The presence of HIF-1 leads to a significant upregulation of the reporter gene expression. HRE-Luciferase reporter constructs have been shown to be valuable tools to evaluate tumor hypoxia and the efficacy of hypoxia directed therapies in vivo (Fig. 5) [61, 62]. Bioluminescence, a process requiring ATP and O_2, did not seem to be hampered by the low oxygen tension in the tissue.

In another approach to visualize hypoxic signaling and HIF-1 stabilization, reporter cell lines, constitutively expressing a fusion protein consisting of the ODD coupled to luciferase, have been generated [65]. Slightly different models are reporter cell lines in which express a HIF-1:luciferase fusion protein [61, 66]. In both reporter cell lines, luciferase will be degraded immediately under normoxic conditions, so no luciferase signal can be detected. Under hypoxic conditions, luciferase will be stabilized in a similar manner as HIF-1 which will result in a detectable signal. These imaging tools are useful for studying the biology of tumor hypoxia and mechanisms of response to experimental antiangiogenic therapy.

Fluorescent probes

In addition to the bioluminescent and fluorescent gene reporter systems discussed above, various fluorescent protease-sensing probes and targeted probes have been developed. The first protease-sensing optical probes were autoquench fluorescent probes that convert from a nonfluorescent to a fluorescent state by proteolytic activation of lysosomal cysteine or serine proteases like cathepsin-B [67]. The utility of these probes has also been extended to other enzymes such as thrombin and matrix metalloproteinase-2 by inserting enzyme-specific peptide stalks between the carrier and the fluorochromes [67–70]. Targeted probes consist of a fluorophore coupled to a highly specific antibody or single chain lama-antibodies, affibodies or ligands.

$\alpha v\beta 3$ targeted probes

The $\alpha_v\beta_3$ integrin plays a crucial role during tumor angiogenesis. It is highly expressed on endothelial cells of newly formed tumor vasculature and on various tumor cells, whereas quiescent endothelial cells and other non-cancerous cells are largely $\alpha_v\beta_3$ negative. The amino acid sequence Arg-Gly-Asp (RGD), also present in matrix molecules like
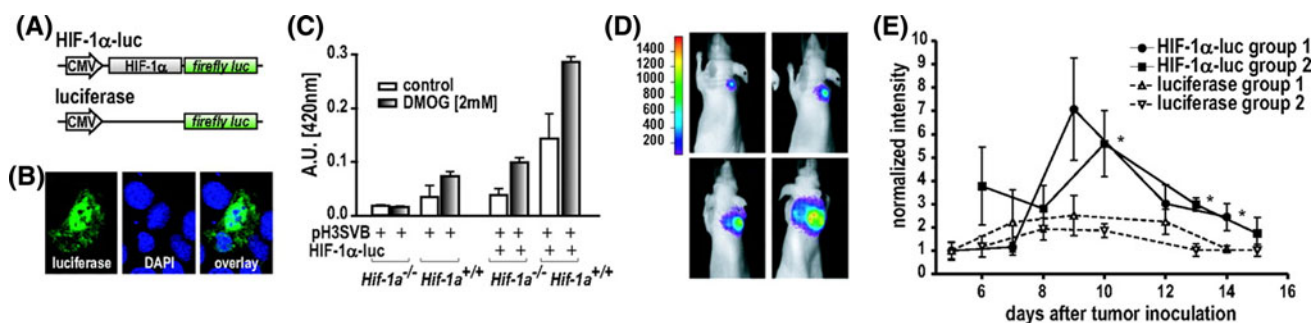

Fig. 5 In vivo monitoring of the stabilization of HIF-1α using bioluminescence imaging. **a** pcDNA3.1-mHIF-1α-luciferase (HIF-1α-luc) and pcDNA3.1-luciferase (luciferase) reporter constructs. **b** Immunofluorescence staining of firefly luciferase in MEF cells transiently transfected with pcDNA3.1-mHIF-1α-luciferase. Nuclei were stained with DAPI. (Magnification: × 300.) **c** Assessment of oxygen-dependent regulation and transcriptional activity of the HIF-1α-luciferase fusion construct. MEF-Hif1a +/+ or MEF-Hif1a −/− were cotransfected with pcDNA3.1 mHIF-1α-luciferase, and the reporter plasmid pH3SVB, which drives the expression of β-galactosidase from a HIF responsive promoter. β-Galactosidase activity was assessed. Data are representative of 2 independent experiments. **d** Bioluminescent images of a mouse carrying a HIF-1α-luciferase C51 tumor in the neck. Four consecutive images of the same animal are shown. *Color bar* indicates total photon counts. **e** Normalized bioluminescence photon counts (mean ± SEM) relative to day 5 values for both the HIF1α-luciferase and the luciferase control tumors. Values indicated by *asterisk* significantly ($P \leq 0.05$) differ from values measured in control groups. (Adapted with permission from Lehmann et al. Proc Natl Acad Sci USA. 2009 Aug 18; 106(33):14004–9. Epub 2009 Jul 31. [61])
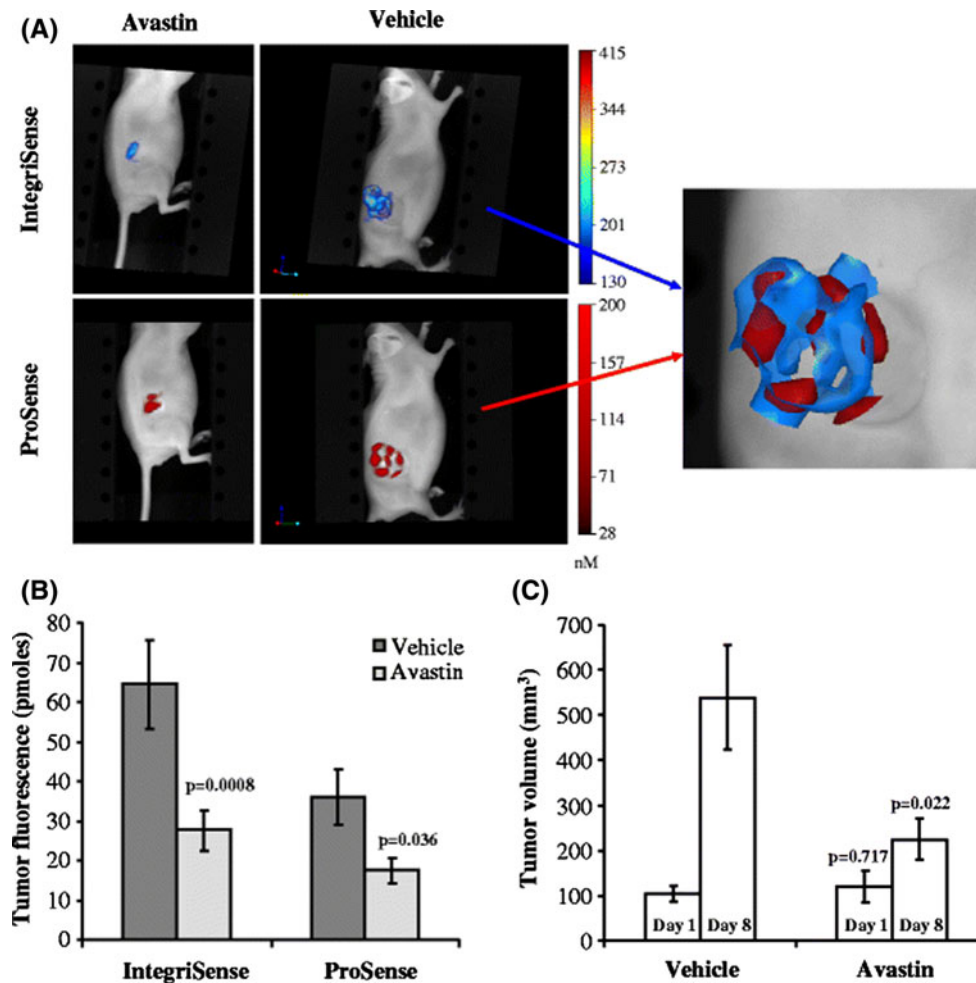
Fig. 6 Effect of antiangiogenic Avastin treatment on $\alpha v\beta 3$ integrin and cathepsin B signals in A673 tumor-bearing mice. **a** Representative volume renderings of IntegriSense and ProSense. Note the differential localization of fluorescent signal with IntegriSense and ProSense in the same animals (IntegriSense in blue and ProSense in red). **b** Quantification of tumor fluorescence shows that IntegriSense and Prosense signal in tumors is decreased following Avastin treatment ($P = 0.0008$ and $P = 0.013$, respectively). **c** Avastin also significantly inhibits tumor growth as determined by tumor volume calipers measurements (by 58.4%, $P = 0.022$). (Reprinted from Kossodo S, Pickarski M, Lin SA, Gleason A, Gaspar R, Buono C, Ho G, Blusztajn A, Cuneo G, Zhang J, Jensen J, Hargreaves R, Coleman P, Hartman G, Rajopadhye M, Duong LT, Sur C, Yared W, Peterson J, Bednar B. Dual In Vivo Quantification of Integrin-targeted and Protease-activated Agents in Cancer Using Fluorescence Molecular Tomography (FMT). Mol Imaging Biol 2009. [87])

vibronectin, is a tripeptide that selectively binds to integrin receptors including $\alpha_v\beta_3$ and $\alpha_v\beta_5$ [71–73]. The activation of $\alpha_v\beta_3$ integrin is not limited to tumor biology and thus probes targeting $\alpha_v\beta_3$ integrin can be a valuable tool to study other processes and diseases as well, for example angiogenesis, atherosclerosis, inflammation, bone remodeling and arthritis.

Based on the binding of RGD to $\alpha_v\beta_3$ integrin, Haubner et al. [74] developed ^{125}I and later [18]F [75] labeled tracers to image $\alpha_v\beta_3$ integrin expression and tumor angiogenesis. In recent years, many fluorescently labeled cyclic RGD peptides have been developed for near infrared fluorescence imaging like RGD-Cy7, RGD-Cy5.5, RGD-QD705 [76–78] and cyclic RGD coupled to IRDye 800CW-labeled peptide which is even more shifted towards the infrared parts of the spectrum resulting in ideal fluorescent

characteristics for in vivo use [79, 80]. Mulder et al. [81, 82] recently described paramagnetic lipid-encapsulated quantum dots with RGD presented at the outside and a green fluorescent quantum dot at the inside of the micellar shell. These targeted particles are both suitable for fluorescence imaging as well as magnetic resonance imaging (MRI), thus providing unique opportunities for the use of multi modality molecular imaging.

Several groups have improved $\alpha_v\beta_3$ integrin specificity, binding affinity, and possible targeted delivery of therapeutics, by coupling multiple RGD motifs on a backbone molecule [81–85]. Although many types of tumor cells are positive for $\alpha_v\beta_3$ integrin, RGD-modified proteins mainly localize at the tumor endothelium and not in the tumor itself [86].
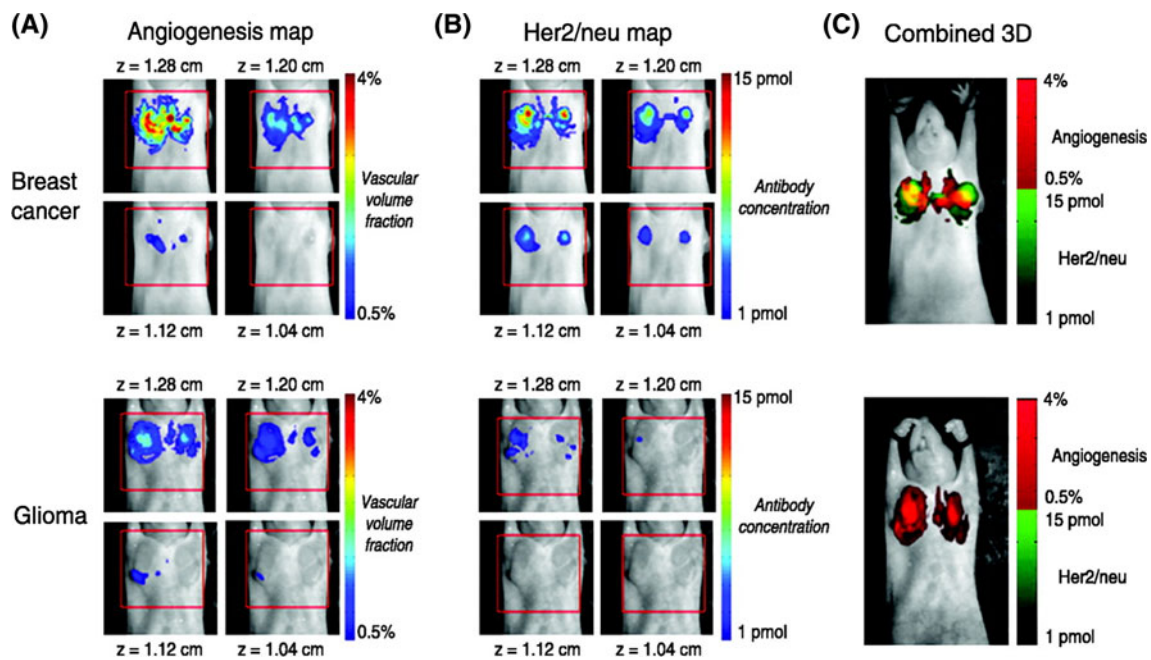
Fig. 7 Dual target imaging. Mice bearing xenograft tumors (either breast cancers or gliosarcomas) were imaged at two different wavelengths to map angiogenesis (**a** 748 nm) and HER-2/*neu* (**b** 672 nm) in the same animal. The gliosarcoma is largely devoid of HER-2/*neu*. **c** a combined three-dimensional map of both processes. (Adapted with permission from Montet et al. Cancer Res. 2005 Jul 15; 65(14):6330–6. Fig. 4 [95])

The commercially available near infrared fluorescent (NIRF) probe IntegriSense (Visen Medical) consists of a small molecule nonpeptide $\alpha_v\beta_3$ antagonist fused to the VivoTag-S680 near infrared fluorophore. IntegriSense has a much higher specificity for $\alpha_v\beta_3$ integrin compared to RGD-based probes. Unlike RGD-based probes, extravasation of IntegriSense does occur and the probe localizes at both at the surface of $\alpha_v\beta_3$ integrin positive endothelial cells and the surface of $\alpha_v\beta_3$ integrin positive tumor cells. Furthermore, IntegriSense is internalized by $\alpha_v\beta_3$ integrin positive tumor cells leading to a slower clearance of the probe from tumors compared to the surrounding tissues. A drawback of the slower clearance from a tumor is the practical upper limit on the possible frequency of repeated measurements [87].

Using fluorescence-mediated tomography (FMT), Kossodo et al. [87] measured tumor volume and vascularization in A673 tumor-bearing mice. They used IntegriSense to visualize blood vessels and ProSense, a cathepsin-based protease activated fluorescent probe which only fluoresces after being cleaved by proteases, to visualize the tumor. In addition they were able to quantify the effect of antiangiogenic treatment (Fig. 6).

VEGF-receptor targeted probes

The VEGFR-2 is a very attractive endothelial target for imaging of tumor angiogenesis due to its temporal and local upregulation during (tumor-)angiogenesis [24–28].

To target the VEGFR-2, Backer et al. [88] used single chain VEGF (scVEGF) with an N-terminal cysteine-containing tag (Cys-tag) which can be used for site specific attachment of various agents [89]. The scVEGF-based family of probes has been validated to target the VEGF receptor in vitro and in vivo tumor angiogenesis [90, 91]. More recently, scVEGF labeled with the near infrared dye Cy5.5 has been used for fluorescence imaging of VEGF receptor in angiogenic vasculature, in regions of sterile inflammation and during tumor angiogenesis [92, 93].

Long circulating fluorescent agents

Long circulating blood pool macromolecules labeled with gadolinium have been used as traditional MRI contrast agent for determining vascular volumes [94]. The rapid advancements in fluorescence imaging lead to the need for long circulating fluorescent agents. The first generation of these fluorescent probes was based on long circulating dextrinated iron oxide (LCDIO) preparations coupled to a fluorescent label [95–97]. These probes were used by Bremer et al. [97] to determine the tumoral vascular volume fractions by MRI validated with fluorescence intravital microscopy.

With the development of FMT for small laboratory animals the imaging focus shifted from intravital microscopy to 3D whole body imaging. Using the commercially available near IR fluorochrome labeled long circulating synthetic graft copolymer AngioSense-750 and the fluorescently labeled

Her2 antibody herceptin (Herceptin-Cy5.5), Montet et al. [95] demonstrated the possibility to co-register angiogenesis and tumor growth with FMT. In their experiment they used a Her2/neu positive breast cancer xenograft model and a glioma model with low expression of Her2/Neu (Fig. 7). In later studies they confirmed that FMT allows quantitative visualization of tumoral vascular volume fractions in mice using Herceptin-Cy5.5, AngioSense-680 and AngioSense-750 [98]. Both AngioSense-680 and AngioSense-750 are fluorescently labeled long circulating synthetic graft copolymers optimized for 680 and 750 nm excitation wavelengths, respectively.

Conclusion and future directions

Here we discussed a great number of optical imaging models that can be used to image the angiogenic process on various levels ranging from intravital microscopy to whole body imaging. The cost effective and non invasive character of optical imaging makes it an ideal imaging modality for repeated measurements and to follow treatment response of anti-angiogenic treatment over time. New imaging systems, that are able to unmix signals of various wavelengths, make it possible to study various fluorescent and luminescent signals simultaneously. This offers a powerful tool to study different processes and interactions, for example tumor growth and angiogenesis, in the same animal. Furthermore, optical imaging can be combined with various other imaging modalities, for example the fluorescent paramagnetic $\alpha_v\beta_3$ targeted probes with MRI contrast that offer the opportunity to image angiogenesis at high resolution with MRI while confirming the specificity of the MRI contrast with the co-localized fluorescent signal. The development of less toxic near infrared fluorescent probes open up the opportunity to apply fluorescence imaging in various clinical settings in the near future.

References

1. Contag CH, Bachmann MH (2002) Advances in in vivo bioluminescence imaging of gene expression. Annu Rev Biomed Eng 4:235–260

2. Bhaumik S, Gambhir SS (2002) Optical imaging of Renilla luciferase reporter gene expression in living mice. Proc Natl Acad Sci USA 99:377–382

3. Hastings JW (1996) Chemistries and colors of bioluminescent reactions: a review. Gene 173:5–11

4. Pichler A, Prior JL, Piwnica-Worms D (2004) Imaging reversal of multidrug resistance in living mice with bioluminescence: MDR1 P-glycoprotein transports coelenterazine. Proc Natl Acad Sci USA 101:1702–1707

5. Tannous BA, Kim DE, Fernandez JL, Weissleder R, Breakefield XO (2005) Codon-optimized Gaussia luciferase cDNA for mammalian gene expression in culture and in vivo. Mol Ther 11:435–443

6. Verhaegent M, Christopoulos TK (2002) Recombinant Gaussia luciferase. Overexpression, purification, and analytical application of a bioluminescent reporter for DNA hybridization. Anal Chem 74:4378–4385

7. Hoffman RM (2005) The multiple uses of fluorescent proteins to visualize cancer in vivo. Nat Rev Cancer 5:796–806

8. Demas JN, Crosby GA (1971) Measurement of photoluminescence quantum yields. A review. J Phys Chem 75:991–1024

9. Weissleder R, Ntziachristos V (2003) Shedding light onto live molecular targets. Nat Med 9:123–128

10. Lim YT, Kim S, Nakayama A, Stott NE, Bawendi MG, Frangioni JV (2003) Selection of quantum dot wavelengths for biomedical assays and imaging. Mol Imaging 2:50–64

11. Giepmans BN, Adams SR, Ellisman MH, Tsien RY (2006) The fluorescent toolbox for assessing protein location and function. Science 312:217–224

12. Shcherbo D, Merzlyak EM, Chepurnykh TV, Fradkov AF, Ermakova GV, Solovieva EA, Lukyanov KA, Bogdanova EA, Zaraisky AG, Lukyanov S, Chudakov DM (2007) Bright far-red fluorescent protein for whole-body imaging. Nat Methods 4:741–746

13. Shaner NC, Campbell RE, Steinbach PA, Giepmans BN, Palmer AE, Tsien RY (2004) Improved monomeric red, orange and yellow fluorescent proteins derived from *Discosoma* sp. red fluorescent protein. Nat Biotechnol 22:1567–1572

14. Wang L, Jackson WC, Steinbach PA, Tsien RY (2004) Evolution of new nonantibody proteins via iterative somatic hypermutation. Proc Natl Acad Sci USA 101:16745–16749

15. Shu X, Royant A, Lin MZ, Aguilera TA, Lev-Ram V, Steinbach PA, Tsien RY (2009) Mammalian expression of infrared fluorescent proteins engineered from a bacterial phytochrome. Science 324:804–807

16. Virostko J, Jansen ED (2009) Validation of bioluminescent imaging techniques. Methods Mol Biol 574:15–23

17. Qin C, Yang X, Feng J, Liu K, Liu J, Yan G, Zhu S, Xu M, Tian J (2009) Adaptive improved element free Galerkin method for quasi- or multi-spectral bioluminescence tomography. Opt Express 17:21925–21934

18. Zhang Q, Yin L, Tan Y, Yuan Z, Jiang H (2008) Quantitative bioluminescence tomography guided by diffuse optical tomography. Opt Express 16:1481–1486

19. Rogers KL, Picaud S, Roncali E, Boisgard R, Colasante C, Stinnakre J, Tavitian B, Brulet P (2007) Non-invasive in vivo imaging of calcium signaling in mice. PLoS One 2:e974

20. Roncali E, Savinaud M, Levrey O, Rogers KL, Maitrejean S, Tavitian B (2008) New device for real-time bioluminescence imaging in moving rodents. J Biomed Opt 13:054035

21. Leblond F, Davis SC, Valdes PA, Pogue BW (2010) Pre-clinical whole-body fluorescence imaging: Review of instruments, methods and applications. J Photochem Photobiol B 98:77–94

22. Mansfield JR, Gossage KW, Hoyt CC, Levenson RM (2005) Autofluorescence removal, multiplexing, and automated analysis methods for in vivo fluorescence imaging. J Biomed Opt 10:41207

23. Levenson RM, Lynch DT, Kobayashi H, Backer JM, Backer MV (2008) Multiplexing with multispectral imaging: from mice to microscopy. ILAR J 49:78–88

24. Millauer B, Wizigmann-Voos S, Schnurch H, Martinez R, Moller NP, Risau W, Ullrich A (1993) High affinity VEGF binding and developmental expression suggest Flk-1 as a major regulator of vasculogenesis and angiogenesis. Cell 72:835–846

25. Couffinhal T, Kearney M, Witzenbichler B, Chen D, Murohara T, Losordo DW, Symes J, Isner JM (1997) Vascular endothelial growth factor/vascular permeability factor (VEGF/VPF) in normal and atherosclerotic human arteries. Am J Pathol 150: 1673–1685

26. Rissanen TT, Vajanto I, Hiltunen MO, Rutanen J, Kettunen MI, Niemi M, Leppanen P, Turunen MP, Markkanen JE, Arve K, Alhava E, Kauppinen RA, Yla-Herttuala S (2002) Expression of vascular endothelial growth factor and vascular endothelial growth factor receptor-2 (KDR/Flk-1) in ischemic skeletal muscle and its regeneration. Am J Pathol 160:1393–1403

27. Vajkoczy P, Farhadi M, Gaumann A, Heidenreich R, Erber R, Wunder A, Tonn JC, Menger MD, Breier G (2002) Microtumor growth initiates angiogenic sprouting with simultaneous expression of VEGF, VEGF receptor-2, and angiopoietin-2. J Clin Invest 109:777–785

28. Witmer AN, Dai J, Weich HA, Vrensen GF, Schlingemann RO (2002) Expression of vascular endothelial growth factor receptors 1, 2, and 3 in quiescent endothelia. J Histochem Cytochem 50:767–777

29. Zhang N, Fang Z, Contag PR, Purchio AF, West DB (2004) Tracking angiogenesis induced by skin wounding and contact hypersensitivity using a Vegfr2-luciferase transgenic mouse. Blood 103:617–626

30. Ronicke V, Risau W, Breier G (1996) Characterization of the endothelium-specific murine vascular endothelial growth factor receptor-2 (Flk-1) promoter. Circ Res 79:277–285

31. Ryan PL, Youngblood RC, Harvill J, Willard ST (2005) Photonic monitoring in real time of vascular endothelial growth factor receptor 2 gene expression under relaxin-induced conditions in a novel murine wound model. Ann NY Acad Sci 1041:398–414

32. Ehrbar M, Zeisberger SM, Raeber GP, Hubbell JA, Schnell C, Zisch AH (2008) The role of actively released fibrin-conjugated VEGF for VEGF receptor 2 gene activation and the enhancement of angiogenesis. Biomaterials 29:1720–1729

33. Morrison BW, Leder P (1994) neu and ras initiate murine mammary tumors that share genetic markers generally absent in c-myc and int-2-initiated tumors. Oncogene 9:3417–3426

34. Kishimoto J, Ehama R, Ge Y, Kobayashi T, Nishiyama T, Detmar M, Burgeson RE (2000) In vivo detection of human vascular endothelial growth factor promoter activity in transgenic mouse skin. Am J Pathol 157:103–110

35. Wang Y, Iyer M, Annala A, Wu L, Carey M, Gambhir SS (2006) Noninvasive indirect imaging of vascular endothelial growth factor gene expression using bioluminescence imaging in living transgenic mice. Physiol Genomics 24:173–180

36. Iyer M, Wu L, Carey M, Wang Y, Smallwood A, Gambhir SS (2001) Two-step transcriptional amplification as a method for imaging reporter gene expression using weak promoters. Proc Natl Acad Sci USA 98:14595–14600

37. Hillen F, Kaijzel EL, Castermans K, oude Egbrink MG, Lowik CW, Griffioen AW (2008) A transgenic Tie2-GFP athymic mouse model; a tool for vascular biology in xenograft tumors. Biochem Biophys Res Commun 368:364–367

38. Motoike T, Loughna S, Perens E, Roman BL, Liao W, Chau TC, Richardson CD, Kawate T, Kuno J, Weinstein BM, Stainier DY, Sato TN (2000) Universal GFP reporter for the study of vascular development. Genesis 28:75–81

39. van Haperen R, Cheng C, Mees BM, van Deel E, de Waard M, van Damme LC, van Gent T, van Aken T, Krams R, Duncker DJ, de Crom R (2003) Functional expression of endothelial nitric oxide synthase fused to green fluorescent protein in transgenic mice. Am J Pathol 163:1677–1686

40. Yang M, Baranov E, Li XM, Wang JW, Jiang P, Li L, Moossa AR, Penman S, Hoffman RM (2001) Whole-body and intravital optical imaging of angiogenesis in orthotopically implanted tumors. Proc Natl Acad Sci USA 98:2616–2621

41. Yang M, Li L, Jiang P, Moossa AR, Penman S, Hoffman RM (2003) Dual-color fluorescence imaging distinguishes tumor cells from induced host angiogenic vessels and stromal cells. Proc Natl Acad Sci USA 100:14259–14262

42. Okabe M, Ikawa M, Kominami K, Nakanishi T, Nishimune Y (1997) 'Green mice' as a source of ubiquitous green cells. FEBS Lett 407:313–319

43. Lendahl U, Zimmerman LB, McKay RD (1990) CNS stem cells express a new class of intermediate filament protein. Cell 60: 585–595

44. Zimmerman L, Parr B, Lendahl U, Cunningham M, McKay R, Gavin B, Mann J, Vassileva G, McMahon A (1994) Independent regulatory elements in the nestin gene direct transgene expression to neural stem cells or muscle precursors. Neuron 12:11–24

45. Yaworsky PJ, Kappen C (1999) Heterogeneity of neural progenitor cells revealed by enhancers in the nestin gene. Dev Biol 205:309–321

46. Li L, Mignone J, Yang M, Matic M, Penman S, Enikolopov G, Hoffman RM (2003) Nestin expression in hair follicle sheath progenitor cells. Proc Natl Acad Sci USA 100:9958–9961

47. Yano K, Brown LF, Detmar M (2001) Control of hair growth and follicle size by VEGF-mediated angiogenesis. J Clin Invest 107:409–417

48. Amoh Y, Li L, Yang M, Moossa AR, Katsuoka K, Penman S, Hoffman RM (2004) Nascent blood vessels in the skin arise from nestin-expressing hair-follicle cells. Proc Natl Acad Sci USA 101:13291–13295

49. Mecklenburg L, Tobin DJ, Muller-Rover S, Handjiski B, Wendt G, Peters EM, Pohl S, Moll I, Paus R (2000) Active hair growth (anagen) is associated with angiogenesis. J Invest Dermatol 114:909–916

50. Amoh Y, Li L, Yang M, Jiang P, Moossa AR, Katsuoka K, Hoffman RM (2005) Hair follicle-derived blood vessels vascularize tumors in skin and are inhibited by Doxorubicin. Cancer Res 65:2337–2343

51. Amoh Y, Yang M, Li L, Reynoso J, Bouvet M, Moossa AR, Katsuoka K, Hoffman RM (2005) Nestin-linked green fluorescent protein transgenic nude mouse for imaging human tumor angiogenesis. Cancer Res 65:5352–5357

52. Amoh Y, Nagakura C, Maitra A, Moossa AR, Katsuoka K, Hoffman RM, Bouvet M (2006) Dual-color imaging of nascent angiogenesis and its inhibition in liver metastases of pancreatic cancer. Anticancer Res 26:3237–3242

53. Amoh Y, Bouvet M, Li L, Tsuji K, Moossa AR, Katsuoka K, Hoffman RM (2006) Visualization of nascent tumor angiogenesis in lung and liver metastasis by differential dual-color fluorescence imaging in nestin-linked-GFP mice. Clin Exp Metastasis 23:315–322

54. Hayashi K, Yamauchi K, Yamamoto N, Tsuchiya H, Tomita K, Amoh Y, Hoffman RM, Bouvet M (2007) Dual-color imaging of angiogenesis and its inhibition in bone and soft tissue sarcoma. J Surg Res 140:165–170

55. Ji Y, Hayashi K, Amoh Y, Tsuji K, Yamauchi K, Yamamoto N, Tsuchiya H, Tomita K, Bouvet M, Hoffman RM (2007) The camptothecin derivative CPT-11 inhibits angiogenesis in a dual-color imageable orthotopic metastatic nude mouse model of human colon cancer. Anticancer Res 27:713–718

56. Bartelle BB, Berrios-Otero C, Friedland AE, Turnbull DH (2009) Transgenic mice for multimodal imaging of angiogenesis. In: 2009 world molecular imaging congress, presentation no. 0146. 25-9-2009. Ref Type: Abstract

57. Liao D, Johnson RS (2007) Hypoxia: a key regulator of angiogenesis in cancer. Cancer Metastasis Rev 26:281–290

58. Gleadle JM (2009) Review article: how cells sense oxygen: lessons from and for the kidney. Nephrology (Carlton) 14:86–93

59. O'Rourke JF, Dachs GU, Gleadle JM, Maxwell PH, Pugh CW, Stratford IJ, Wood SM, Ratcliffe PJ (1997) Hypoxia response elements. Oncol Res 9:327–332

60. Shibata T, Giaccia AJ, Brown JM (2000) Development of a hypoxia-responsive vector for tumor-specific gene therapy. Gene Ther 7:493–498

61. Lehmann S, Stiehl DP, Honer M, Dominietto M, Keist R, Kotevic I, Wollenick K, Ametamey S, Wenger RH, Rudin M (2009) Longitudinal and multimodal in vivo imaging of tumor hypoxia and its downstream molecular events. Proc Natl Acad Sci USA 106:14004–14009

62. Harada H, Kizaka-Kondoh S, Hiraoka M (2005) Optical imaging of tumor hypoxia and evaluation of efficacy of a hypoxia-targeting drug in living animals. Mol Imaging 4:182–193

63. Vordermark D, Shibata T, Brown JM (2001) Green fluorescent protein is a suitable reporter of tumor hypoxia despite an oxygen requirement for chromophore formation. Neoplasia 3:527–534

64. Brader P, Riedl CC, Woo Y, Ponomarev V, Zanzonico P, Wen B, Cai S, Hricak H, Fong Y, Blasberg R, Serganova I (2007) Imaging of hypoxia-driven gene expression in an orthotopic liver tumor model. Mol Cancer Ther 6:2900–2908

65. Li F, Sonveaux P, Rabbani ZN, Liu S, Yan B, Huang Q, Vujaskovic Z, Dewhirst MW, Li CY (2007) Regulation of HIF-1alpha stability through S-nitrosylation. Mol Cell 26:63–74

66. Moroz E, Carlin S, Dyomina K, Burke S, Thaler HT, Blasberg R, Serganova I (2009) Real-time imaging of HIF-1alpha stabilization and degradation. PLoS One 4:e5077

67. Weissleder R, Tung CH, Mahmood U, Bogdanov A Jr (1999) In vivo imaging of tumors with protease-activated near-infrared fluorescent probes. Nat Biotechnol 17:375–378

68. Bremer C, Tung CH, Weissleder R (2001) In vivo molecular target assessment of matrix metalloproteinase inhibition. Nat Med 7:743–748

69. Bremer C, Bredow S, Mahmood U, Weissleder R, Tung CH (2001) Optical imaging of matrix metalloproteinase-2 activity in tumors: feasibility study in a mouse model. Radiology 221:523–529

70. Marten K, Bremer C, Khazaie K, Sameni M, Sloane B, Tung CH, Weissleder R (2002) Detection of dysplastic intestinal adenomas using enzyme-sensing molecular beacons in mice. Gastroenterology 122:406–414

71. Griffioen AW, Molema G (2000) Angiogenesis: potentials for pharmacologic intervention in the treatment of cancer, cardiovascular diseases, and chronic inflammation. Pharmacol Rev 52:237–268

72. Brooks PC, Clark RA, Cheresh DA (1994) Requirement of vascular integrin alpha v beta 3 for angiogenesis. Science 264:569–571

73. Xiong JP, Stehle T, Zhang R, Joachimiak A, Frech M, Goodman SL, Arnaout MA (2002) Crystal structure of the extracellular segment of integrin alpha Vbeta3 in complex with an Arg-Gly-Asp ligand. Science 296:151–155

74. Haubner R, Wester HJ, Reuning U, Senekowitsch-Schmidtke R, Diefenbach B, Kessler H, Stocklin G, Schwaiger M (1999) Radiolabeled alpha(v)beta3 integrin antagonists: a new class of tracers for tumor targeting. J Nucl Med 40:1061–1071

75. Haubner R, Wester HJ, Weber WA, Mang C, Ziegler SI, Goodman SL, Senekowitsch-Schmidtke R, Kessler H, Schwaiger M (2001) Noninvasive imaging of alpha(v)beta3 integrin expression

using 18F-labeled RGD-containing glycopeptide and positron emission tomography. Cancer Res 61:1781–1785

76. Wu Y, Cai W, Chen X (2006) Near-infrared fluorescence imaging of tumor integrin alpha v beta 3 expression with Cy7-labeled RGD multimers. Mol Imaging Biol 8:226–236

77. Cai W, Shin DW, Chen K, Gheysens O, Cao Q, Wang SX, Gambhir SS, Chen X (2006) Peptide-labeled near-infrared quantum dots for imaging tumor vasculature in living subjects. Nano Lett 6:669–676

78. Chen X, Conti PS, Moats RA (2004) In vivo near-infrared fluorescence imaging of integrin alphavbeta3 in brain tumor xenografts. Cancer Res 64:8009–8014

79. Adams KE, Ke S, Kwon S, Liang F, Fan Z, Lu Y, Hirschi K, Mawad ME, Barry MA, Sevick-Muraca EM (2007) Comparison of visible and near-infrared wavelength-excitable fluorescent dyes for molecular imaging of cancer. J Biomed Opt 12:024017

80. Kovar J, Kovar J, Boveia V, Boveia V, Chen H, Chen H, Peng X, Peng X, Skopp R, Skopp R, Little G, Little G, Draney D, Draney D, Olive DM, Olive DM (2009) Near infrared probes for biochemical, cellular, and whole animal analysis of disease processes. Proc SPIE 7190:71900N

81. Mulder WJ, Koole R, Brandwijk RJ, Storm G, Chin PT, Strijkers GJ, de Mello DC, Nicolay K, Griffioen AW (2006) Quantum dots with a paramagnetic coating as a bimodal molecular imaging probe. Nano Lett 6:1–6

82. Mulder WJ, Castermans K, van Beijnum JR, oude Egbrink MG, Chin PT, Fayad ZA, Lowik CW, Kaijzel EL, Que I, Storm G, Strijkers GJ, Griffioen AW, Nicolay K (2009) Molecular imaging of tumor angiogenesis using alphavbeta3-integrin targeted multimodal quantum dots. Angiogenesis 12:17–24

83. Cheng Z, Wu Y, Xiong Z, Gambhir SS, Chen X (2005) Near-infrared fluorescent RGD peptides for optical imaging of integrin alphavbeta3 expression in living mice. Bioconjug Chem 16:1433–1441

84. Jin ZH, Josserand V, Foillard S, Boturyn D, Dumy P, Favrot MC, Coll JL (2007) In vivo optical imaging of integrin alphaV-beta3 in mice using multivalent or monovalent cRGD targeting vectors. Mol Cancer 6:41

85. Kok RJ, Schraa AJ, Bos EJ, Moorlag HE, Asgeirsdottir SA, Everts M, Meijer DK, Molema G (2002) Preparation and functional evaluation of RGD-modified proteins as alpha(v)beta(3) integrin directed therapeutics. Bioconjug Chem 13:128–135

86. Schraa AJ, Kok RJ, Moorlag HE, Bos EJ, Proost JH, Meijer DK, de Leij LF, Molema G (2002) Targeting of RGD-modified proteins to tumor vasculature: a pharmacokinetic and cellular distribution study. Int J Cancer 102:469–475

87. Kossodo S, Pickarski M, Lin SA, Gleason A, Gaspar R, Buono C, Ho G, Blusztajn A, Cuneo G, Zhang J, Jensen J, Hargreaves R, Coleman P, Hartman G, Rajopadhye M, Duong LT, Sur C, Yared W, Peterson J, Bednar B (2009) Dual in vivo quantification of integrin-targeted and protease-activated agents in cancer using fluorescence molecular tomography (FMT). Mol Imaging Biol

88. Backer MV, Patel V, Jehning BT, Claffey KP, Backer JM (2006) Surface immobilization of active vascular endothelial growth factor via a cysteine-containing tag. Biomaterials 27:5452–5458

89. Backer MV, Levashova Z, Levenson R, Blankenberg FG, Backer JM (2008) Cysteine-containing fusion tag for site-specific conjugation of therapeutic and imaging agents to targeting proteins. Methods Mol Biol 494:275–294

90. Blankenberg FG, Backer MV, Levashova Z, Patel V, Backer JM (2006) In vivo tumor angiogenesis imaging with site-specific labeled (99 m)Tc-HYNIC-VEGF. Eur J Nucl Med Mol Imaging 33:841–848

91. Levashova Z, Backer M, Backer JM, Blankenberg FG (2008) Direct site-specific labeling of the Cys-tag moiety in scVEGF with technetium 99 m. Bioconjug Chem 19:1049–1054

92. Levashova Z, Backer M, Backer JM, Blankenberg FG (2009) Imaging vascular endothelial growth factor (VEGF) receptors in turpentine-induced sterile thigh abscesses with radiolabeled single-chain VEGF. J Nucl Med 50:2058–2063

93. Backer MV, Levashova Z, Patel V, Jehning BT, Claffey K, Blankenberg FG, Backer JM (2007) Molecular imaging of VEGF receptors in angiogenic vasculature with single-chain VEGF-based probes. Nat Med 13:504–509

94. Lewin M, Bredow S, Sergeyev N, Marecos E, Bogdanov A Jr, Weissleder R (1999) In vivo assessment of vascular endothelial growth factor-induced angiogenesis. Int J Cancer 83:798–802

95. Montet X, Ntziachristos V, Grimm J, Weissleder R (2005) Tomographic fluorescence mapping of tumor targets. Cancer Res 65:6330–6336

96. Denis MC, Mahmood U, Benoist C, Mathis D, Weissleder R (2004) Imaging inflammation of the pancreatic islets in type 1 diabetes. Proc Natl Acad Sci USA 101:12634–12639

97. Bremer C, Mustafa M, Bogdanov A Jr, Ntziachristos V, Petrovsky A, Weissleder R (2003) Steady-state blood volume measurements in experimental tumors with different angiogenic burdens a study in mice. Radiology 226:214–220

98. Montet X, Figueiredo JL, Alencar H, Ntziachristos V, Mahmood U, Weissleder R (2007) Tomographic fluorescence imaging of tumor vascular volume in mice. Radiology 242:751–758